Structural Effects of Protein Lipidation as Revealed by Lys^{B29}-myristoyl, des(B30) Insulin

Helle B. Olsen and Niels C. Kaarsholm*

Health Care Discovery, Novo Nordisk A/S, Novo Alle 6B1, DK-2880 Bagsvaerd, Denmark

Received May 25, 2000; Revised Manuscript Received July 26, 2000

ABSTRACT: Intracellular proteins are frequently modified by covalent addition of lipid moieties such as myristate. Although a functional role of protein lipidation is implicated in diverse biological processes, only a few examples exist where the structural basis for the phenomena is known. We employ the insulin molecule as a model to evaluate the detailed structural effects induced by myristoylation. Several lines of investigation are used to characterize the solution properties of Lys^{B29}(N^{ϵ}-myristoyl) des(B30) insulin. The structure of the polypeptide chains remains essentially unchanged by the modification. However, the flexible positions taken up by the hydrocarbon chain selectively modify key structural properties. In the insulin monomer, the myristoyl moiety binds in the dimer interface and modulates protein−protein recognition events involved in insulin dimer formation and receptor binding. Myristoylation also contributes stability expressed as an 30% increase in the free energy of unfolding of the protein. Addition of two Zn^{2+}/hexamer and phenol results in the displacement of the myristoyl moiety from the dimer interface and formation of stable R_6 hexamers similar to those formed by human insulin. However, in its new position on the surface of the hexamer, the fatty acid chain affects the equilibria of the phenol-induced interconversions between the T_6, T_3R_3, and R_6 allosteric states of the insulin hexamer. We conclude that insulin is an attractive model system for analyzing the diverse structural effects induced by lipidation of a compact globular protein.

Intracellular peptides and proteins are frequently modified by covalent addition of lipid moieties. The most widely studied of these modifications include attachment of fatty acids (myristate and palmitate), isoprenoids (farnesol and geranylgeranol), and glycophospholipids (glycophosphatidylinositol, GPI)[1] (*1*). On a quantitative basis, it has been estimated that 10−50% of all proteins within mamalian cells may be co- or posttranslationally modified by at least one of these lipids (*2*).

Despite the prevelance of these modifications, in many cases neither the enzymes responsible for the modifications nor the biological role(s) of the modification itself is known. Nevertheless, a functional role of protein lipidation has been implicated in biological processes as diverse as signal transduction and growth regulation, intracellular vesicular transport, cytoskeletal organization, membrane targeting and turnover, as well as replication strategies of patogenic organisms (*3*).

The effects of lipid modification on protein structure are often difficult to access at the molecular level. Due to the lack of an appropriate model system, the roles played of the lipid moiety in modulating properties such as protein−protein interactions, allosteric conformational changes, and protein folding have not been studied in much detail.

Herein we use insulin as such a model system to examine in detail the structural effects elicited by myristoylation of a small globular protein. Insulin consists of two polypeptide chains, an A-chain of 21 amino acids and a B-chain of 30 amino acids. The utility of the molecule as a model system is based on its well-characterized structure and physical biochemical properties. In the monomeric state, the three-dimensional structure of insulin has been determined by NMR spectroscopy (*4*, *5*), and its folding-unfolding transitions have been described (*6*). The protein−protein interactions involved in the formation of insulin dimers and two-zinc insulin hexamers have been characterized by X-ray crystallography (*7*−*9*). Furthermore, the mechanism of ligand induced transitions between the three allosteric forms of the hexamer (the T_6, T_3R_3, and R_6 states, respectively) has been studied in detail (*10*−*13*). In each of these hexamer structures, the A-chain consists of helix (A2−A8), loop (A9−A12), and helix (A14−A20), while the B-chain can assume two principal conformations: In the T-state, the B-chain is composed of N-terminal arm (B1−B8), helix (B9−B19), and β-strand (B22−B28). In the R-state, residues B1−B8 take up a helical conformation to form a region of helix contigous from B1−B19.

Although insulin is biologically active and binds to its cell surface receptor as the monomeric species, the assembly into dimers and various hexameric forms readily takes place in solution. Indeed, the zinc-hexamer is thought to be the storage form of insulin in the pancreas. Consequently, the self-association processes linking the insulin monomer and two-zinc hexamers are important for stable storage and timely

* To whom correspondence should be addressed. E-mail: nck@novo.dk. Fax: +45 4444 4256. Phone: +45 4442 2832.

[1] Abbreviations: GPI, glycophosphatidylinositol; ANS, 1-anilinonaphthalene-8-sulfonic acid; GuHCl, guanidinium hydrochloride; Lys^{B29}-acylated or -myristoylated insulin, Lys^{B29}(N^{ϵ}-tetradecanoyl) des(B30) insulin; TOCSY, total correlation spectroscopy.

10.1021/bi001201i CCC: $19.00
Published on Web 09/07/2000

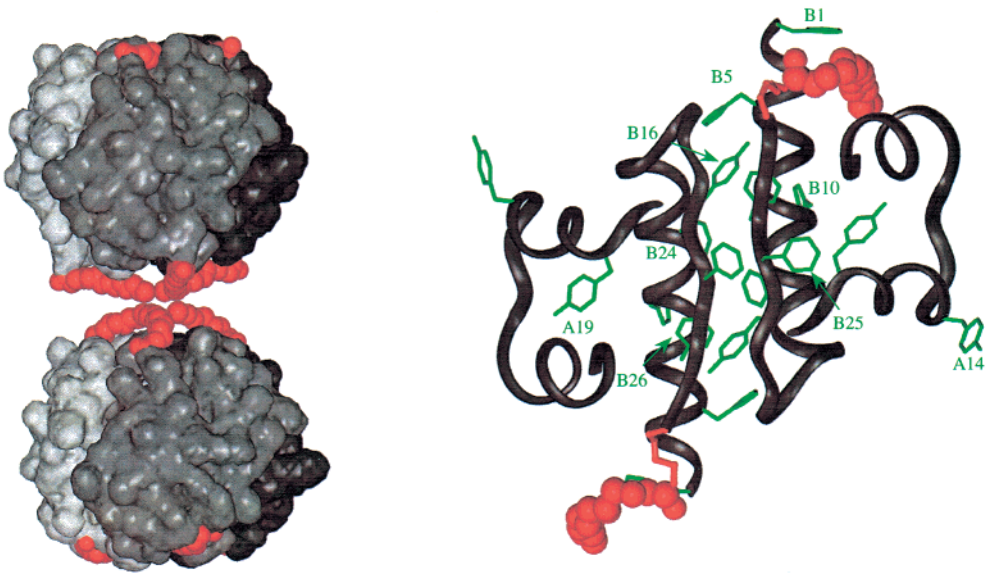

FIGURE 1: X-ray structure of Lys^{B29}-myristoylated insulin (PDB code 1XDA) crystallized in the R_6 state in the presence of Zn^{2+} and phenol. The left panel shows two insulin hexamers with each dimer colored white, gray and black, respectively. The myristate moieties (red) are positioned between hexamers (which are pulled apart for clarity). The right panel shows an insulin dimer in ribbon presentation. The aromatic side chains are shown in green. Note that Tyr^{B16} is buried in the dimer interface together with the Phe^{B24}−Phe^{B25}−Tyr^{B26} sequence which form an antiparallel β-sheet with the inverse sequence of the opposing monomer.

release from the pancreatic β-cells in vivo as well as for the preparation of stable insulin formulations for the treatment of diabetes mellitus (*14*).

The model system to evaluate structural effects of lipidation employs myristoylation of the N^{ϵ}-amino group of the C-terminal B29 Lysine residue of des(B30) insulin, i.e., Lys^{B29}(tetradecanoyl) des(B30) insulin, or simply Lys^{B29}-myristoylated insulin. This derivative was originally prepared to introduce albumin binding properties to the insulin molecule in an effort to slow the release following subcutaneous injection (*15*).

Lys^{B29}-myristoylated insulin has been found to crystallize in the presence of zinc and phenol to form R_6 hexamers. The X-ray structure shows that the conformation of the A- and B-chains of the myristoylated derivative is essentially identical to those of the R_6 hexamers of native human insulin. The fatty acids can be seen bound between hexamers (Figure 1), making specific interactions with the side chains of several residues, in particular Phe^{B1} from the adjacent hexamer. Because the effect of the modification is mostly seen in hexamer−hexamer interactions, Whittingham et al. (*16*) conclude that the mode of binding of the fatty acids appears to be determined by crystal packing.

Herein we show that, although the structure of the polypeptide chains per se remains unchanged, myristoylation modulates a series of structural properties of the insulin molecule in solution. The affected parameters include folding stability, protein−protein interactions in insulin dimerization, and receptor binding as well as ligand induced allosteric conformational transitions in the hexameric state.

EXPERIMENTAL PROCEDURES

Materials. Native human insulin and des(B30)-insulin were supplied by Novo Nordisk A/S. Lys^{B29}(tetradecanoyl) des(B30) insulin was prepared as described (*15*). The C-terminal Thr^{B30} residue is disordered in essentially all the insulin X-ray and NMR structures reported to date and removal of the residue has no effect on the biological activity of human insulin. All other chemicals used in these studied were reagent grade or better.

UV−Vis Spectroscopy. Spectra were collected with an Uvikon 922 spectrophotometer. Protein concentrations were determined by UV-absorbance using $\epsilon_{276} = 6200\ M^{-1}\ cm^{-1}$.

Circular Dichroism Spectroscopy. Far- and near-UV CD spectra were recorded at 20 °C using a Jasco J-715 spectropolarimeter calibrated with (+)-10-camphorsulfonic acid. The CD is expressed as $\Delta\epsilon$ ($M^{-1}\ cm^{-1}$) normalized to the molar concentration of protein and peptide bond, respectively, in the near (250−350 nm)- and far-UV (180−260 nm) ranges.

Guanidine Hydrochloride (GuHCl)-Induced Protein Denaturation. The GuHCl induced unfolding was measured by far-UV CD as described (*6*). The denaturation curves were analyzed by assuming that the folding/unfolding transition is two-state (*17*) and the relationship between the observed $\Delta\epsilon$ and [GuHCl] for the complete unfolding curve is given by the following equation (*18*):

$$\Delta\epsilon = \{(\Delta\epsilon_N^0 + m_N[\mathrm{GuHCl}]) + (\Delta\epsilon_U^0 + m_U[\mathrm{GuHCl}])\exp(-(\Delta G_{H_2O} - m[\mathrm{GuHCl}])/RT)\}/\{1 + \exp(-(\Delta G_{H_2O} - m[\mathrm{GuHCl}])/RT)\} \quad (1)$$

where $\Delta\epsilon_N^0 + m_N[\mathrm{GuHCl}]$ and $\Delta\epsilon_U^0 + m_U[\mathrm{GuHCl}]$ represent the linear dependence of the CD on [GuHCl] in the pre- and posttranslational parts of the unfolding curve, respectively. We assume a linear dependence of ΔG on denaturant concentration: $\Delta G = \Delta G_{H_2O} - m[\mathrm{GuHCl}]$, where ΔG_{H_2O} is the value of ΔG in the absence of denaturant, and m is a measure of the dependence of ΔG on denaturant concentration. Hence, ΔG values derived from K in the transition zone may be extrapolated back to 0 M denaturant to give ΔG_{H_2O} (*18*). The [GuHCl] corresponding to half the population being unfolded, C_{mid}, is given by $\Delta G_{H_2O}/m$.

$T_6 \rightleftarrows T_3R_3 \rightleftarrows R_6$ Transitions. The allosteric conformational changes of the insulin hexamer were followed by the 251 nm CD-signature (*19*), which mainly originates from the disulfide chromophore. The titration experiments employed successive additions of a concentrated phenol stock to a 0.1 cm cuvette containing a solution of 0.6 mM insulin with 2 zinc/hexamer in 10 mM Tris/ClO_4^-, pH 8.0. Blank titrations were subtracted and the resulting $\Delta\epsilon_{251nm}$ vs [phenol] data were converted to the fraction of R-state, ρ, vs [phenol] by dividing the CD at each point by the total change in CD at saturation.

The titration isotherms were fitted to the three-state allosteric model developed by Bloom et al. (*12*). Briefly, the model utilizes four variables to quantitatively describe the homotropic and heterotropic interactions that modulate these transitions. The equilibration of the three hexameric conformations is described by two allosteric constants, $L_0^A = [T_6]/[T_3R_3]$ and $L_0^B = [T_3R_3]/[R_6]$, while ligand (P) binding to the phenolic pockets of T_3R_3 and R_6 is described by dissociation constants, $K_R^0 = [P][T_3R_3]/[T_3R_3P_1]$ and $K_R = [P][R_6]/[R_6P_1]$. The relationship between the model and the symmetry/asymmetry properties of the insulin hexamer is described elsewhere (*11*, *12*, *20*). By setting $\alpha = [P]/K_R$ and $\beta = [P]/K_R^0$, the equation for the fraction of R-state becomes

$$\rho = \frac{0.5L_0^B(1+\beta)^3 + (1+\alpha)^6}{L_0^B(1+\beta)^3 + (1+\alpha)^6 + L_0^B L_0^A} \qquad (2)$$

Fluorescence Spectroscopy. A Perkin-Elmer LS 50B luminescence spectrometer was used to record fluorescence intensities at 20 °C in 1 × 1 cm cuvettes. Fluorescence emission spectra of of 1-anilino-8-naphthalenesulfonate (ANS) were recorded over the range 450−550 nm, and excitation was effected at 415 nm to minimize inner filter effects. When the experiments required that measurements be made under conditions where the inner filter effects become significant, emperically determined calibration curves were used to correct the observed fluorescence. When appropriate, the fluorescence increase was fitted to the following one-site binding equation:

$$F = F_{max}\frac{([P] + [L] + K_d) - \sqrt{([P] + [L] + K_d)^2 - (4[P][L])}}{2[P]} \qquad (3)$$

where [P] and [L] are total concentrations of insulin and ANS, respectively.

NMR Spectroscopy. One-dimensional ^1H and two-dimensional ^1H-^1H NMR spectra were recorded at 600 MHz using a Varian Inova as described (*5*).

RESULTS

Effect of Lys^{B29}-Acylation on the Formation of Insulin Dimer Interface. The pH- and concentration-dependent self-association into dimers and higher aggregates is a hallmark of insulin behavior in solution. In water or dilute buffer, pH 7−8, insulin exists mainly as monomers at concentrations in the low micromolar range. With increasing concentration, dimers and higher aggregates gradually form, while adjustment of the pH toward the alkaline generally shifts the equilibria in the direction of dissociation. Near-UV circular dichroism (CD) and NMR line widths were used to assess the effect of Lys^{B29}-acylation on the self-association properties of insulin in the neutral to weakly alkaline pH-range. The near-UV CD spectrum (250−350 nm) reflects the environments of the tyrosine chromophores. The spectrum is very sensitive to self-association and may be used to monitor the formation of dimer interface.

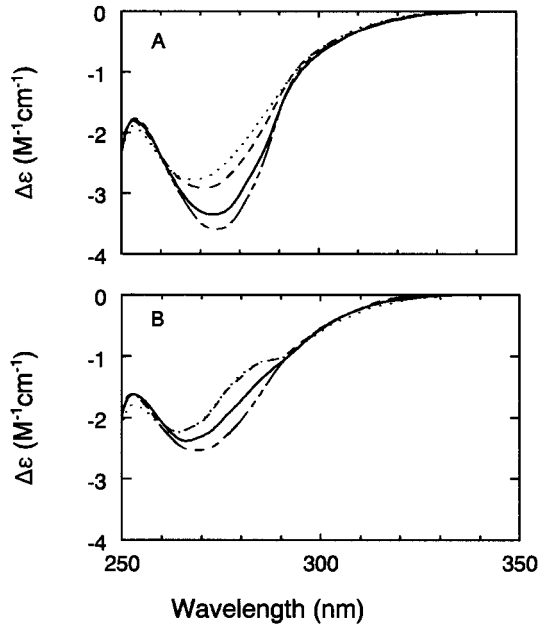

FIGURE 2: Near-UV CD spectra as a function of protein concentration in 10 mM Tris/ClO_4^-, pH 8.0. (A) Zinc-free human insulin at (•••) 5 μM, (− − −) 16 μM, (—) 80 μM, and (- - • - -) 403 μM. (B) Zinc-free Lys^{B29}-myristoylated insulin at (•••) 6 μM, (- - -) 19 μM, (—) 92 μM, and (- - • - -) 464 μM.

Figure 2A shows near-UV CD spectra of zinc-free insulin at variable concentration, pH 8. The dimer exhibits a negative band with minimum located around 273 nm. Dilution leads to a gradual loss of intensity of the band and a blue-shift of the minimum until the monomeric state is reached at a concentration of about 5 μM under these conditions. The corresponding experiment for the acylated protein (Figure 2B) shows that the concentration dependent enhancement of the negative band is retained. However, the effect of increasing protein concentration is significantly weaker and the monomeric state is reached at 19 μM protein. The spectrum of the acylated monomer also has a shoulder at 290 nm, which is absent from the spectrum of the native insulin monomer. These data show that the acyl side chain interferes with dimer formation and affects the chiral environment of at least one tyrosine residue in the monomeric state.

1D ^1H NMR spectra are useful to qualitatively evaluate the presence of insulin self-association because longer rotational correlation times lead to line broadening and because the dynamic equilibria between oligomeric states can lead to line broadening in the intermediate-exchange regime (*5*). Figure 3 compares the concentration dependencies of the aromatic and amide proton resonances of the ^1H NMR spectra for human insulin and the Lys^{B29}-acylated species in 5 mM borate buffer, pH 9.2. This slightly alkaline

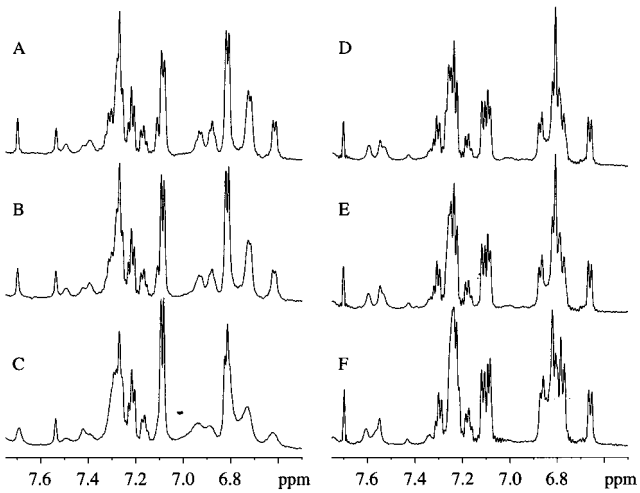

FIGURE 3: 1D NMR spectra showing the aromatic and amide proton resonances as a function of protein concentration in 5 mM borate buffer, pH 9.2, 10/90% D_2O/H_2O, 27 °C. Panels A−C human insulin at 25, 50, and 200 μM, respectively. Panels D−F Lys^{B29}-myristoylated insulin at 25, 50, and 200 μM, respectively.

pH was selected to be able to observe the 1D NMR spectrum of the native monomeric species. As expected, the resolution of the human insulin spectrum (panel A−C) is strongly dependent on protein concentration. The poor resolution at 200 μM (panel C) is improved upon dilution and the spectrum at 25 μM (panel A) exhibits the resolution and dispersion of resonances characteristic of the native insulin monomer (*5*). In contrast, panels D−F show that the spectrum of the Lys^{B29}-acylated insulin remains well-resolved over the entire 25−200 μM range. Again, these data demonstrate that the acyl side-chain interferes with protein−protein recognition in the dimer interface. The net effect is an increase in the dimer dissociation constant of 1 order of magnitude (or more) under these conditions.

Effect of Lys^{B29}-Acylation on Insulin Monomer Structure. Due to extensive self-association (or precipitation) under the conditions normally used for protein solution structure determination by NMR (e.g., 1 mM protein, pH 2−7), a full determination of the NMR-derived structures of insulin and the Lys^{B29}-myristoylated derivative in the monomeric states is not possible. Furthermore, no discrete resonances originating from the myristoyl protons are observed in the aliphatic region of the 1D NMR spectrum of the monomeric derivative indicating that these resonances are likely broadened by exchange between two or more positions on the surface of the insulin molecule. Nevertheless, the 2D TOCSY spectra reveal distinct signatures of the myristoyl moiety as shown in Figures 4 and 5.

Figure 4 compares the aromatic region of 2D TOCSY spectra for insulin and the Lys^{B29}-acylated species both in the monomeric state. As shown in Figure 1, the aromatic residues of insulin are scattered over the molecule. However, several of these form part of the dimer interface, notably Tyr^{B16} of the central B-chain helix and the Phe^{B24}−Phe^{B25}−Tyr^{B26} segment which forms an antiparallel β-sheet with the contiguous Tyr^{B26}−Phe^{B25}−Phe^{B24} segment of the opposing monomer. Therefore, the aromatic region of the spectrum provides a signature of both the dimer interface and the overall structural integrity of the monomer. Figure 4 shows that the aromatic regions of the NMR spectra for the two

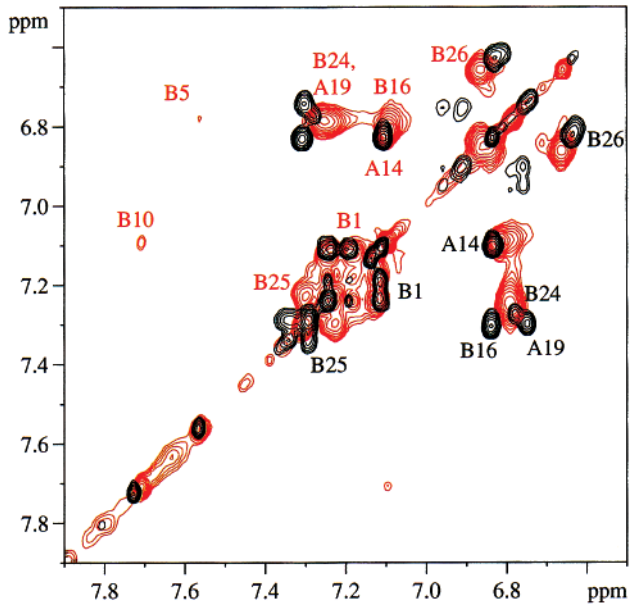

FIGURE 4: Aromatic regions of TOCSY spectra of 25 μM human insulin (black) and 200 μM Lys^{B29}-myristoylated insulin (red) in 5 mM borate buffer, pH 9.2, 27 °C. The annotated cross-peaks show a large change in chemical shift value of TyrB16, while smaller changes are observed for PheB24, PheB25, TyrB26, and TyrA19. The chemical shift values of the remaining aromatic residues are essentially unaffected by Lys^{B29}-acylation. Note that the signals from His^{B5} and His^{B10} are below the lowest contouring level in the spectrum of human insulin.

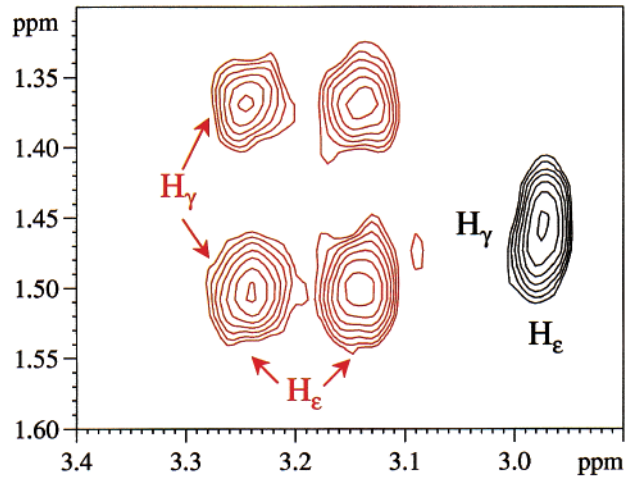

FIGURE 5: Section of TOCSY spectra of 25 μM human insulin (black) and 200 μM Lys^{B29}-myristoylated insulin (red) in 5 mM borate buffer, pH 9.2, 27 °C, showing parts of the Lys^{B29} spin system. The chemical shifts of the γ- and ϵ-methylene proton resonances which are degenerate in native insulin split up upon myristoylation of Lys^{B29}.

proteins are very similar overall. However, there is a relatively large change in the chemical shift value of Tyr^{B16} as a result of acylation. The chemical shift values of residues Phe^{B24}, Phe^{B25}, Tyr^{B26}, and Tyr^{A19} are affected to a smaller extent, while the magnetic environment of the remaining residues (i.e., Phe^{B1}, His^{B5}, His^{B10}, and Tyr^{A14}) is essentially unchanged by myristoylation of Lys^{B29}. Due to the selective perturbation of chemical shift values for the aromatic residues, we conclude that in monomeric Lys^{B29}-acylated insulin, the myristoyl group resides in or close to the putative dimer interface. This finding immediately explains the interference with dimer formation, cf. Figures 2 and 3. Since

portions of the dimer interface overlap with the surface required for recognition of the insulin receptor, e.g., the B24−B26 cluster positioned very close to the affected Tyr^{B16} residue, our data also provide a reasonable explanation for the reduction of at least 50% in receptor binding affinity reported for the Lys^{B29}-myristoylated species (*21*).

The most distinct effect of Lys^{B29}-acylation on the TOCSY spectrum of monomeric insulin is observed for the spin system of the Lys^{B29} side chain carrying the myristoyl group. In all insulin monomers so far examined by NMR spectroscopy, the chemical shift values for the three sets of Lys^{B29} γ-, ϵ-, and δ-methylene protons are each degenerate to random coil values indicating that these proton pairs are solvated. As illustrated for the γ- and ϵ-protons in Figure 5, myristoylation of Lys^{B29} causes the methylene proton pairs to split into separate resonances accompanied by a slight broadening of the signals. This observation is consistent with the Lys^{B29} side chain taking up a defined position at the surface of the monomeric derivative as opposed to the random, fully solvated position taken up in the native monomer. Interestingly, the apparent better definition of the Lys^{B29} side chain is not accompanied by discrete resonances from the myristoyl protons.

Interaction of Lys^{B29}-Myristoylated Insulin with ANS. The presence of the myristoyl group in the putative dimer interface of the insulin monomer should increase the solvent-accessible hydrophobic surface area of the modified insulin monomer. To further characterize this arrangement we examined the interaction of insulin and Lys^{B29}-acylated insulin with the fluorescent dye 1-anilinonaphthalene-8-sulfonate (ANS) at pH 8.0. The fluorescent emission properties of ANS are affected by the polarity of its local environment. A decrease in the polarity of the environment leads to an increase in the quantum yield of ANS while the wavelength of its emission maximum decreases (*22*).

Figure 6A shows the fluorescence spectra of 250 μM ANS alone and in the presence of 80 μM insulin and Lys^{B29}-myristoylated insulin, respectively, at pH 8.0. Under these conditions, we observe a modest increase in the ANS quantum yield and a change in the emission maximum from 516 nm (ANS alone) to 500 nm for native insulin indicative of a relatively weak interaction. Conversely, for the myristoylated species we observe a large increase in quantum yield of ANS and a change in the emission maximum to 481 nm. These data show that Lys^{B29}-myristoylation of insulin greatly enhances the affinity for ANS. Figure 6B shows isotherms for the binding of ANS to various concentrations of Lys^{B29}-myristoylated insulin.The data are consistent with the binding to a single class of sites with an apparent K_d of about 3×10^{-4} M^{-1}.

Effect of Lys^{B29}-Myristoylation on the Folding Stability of Insulin. The contribution of Lys^{B29}-myristoylation to the stability of the insulin fold was examined by guanidine hydrochloride (GuHCl) induced denaturation under conditions where both proteins exists as monomers. For the native insulin monomer, the unfolding transition detected by far-UV CD is characterized by a relatively low degree of cooperativity. Nevertheless, the transition is reasonably described on the basis of a two-state denaturation scheme. The resulting ΔG_{H_2O} value of 3.8 kcal/mol is on the low side for a typical globular protein (*6*). Figure 7 shows that Lys^{B29}-myristoylation leads to a substantial increase in folding stability. The shape of the unfolding curve is essentially unchanged and the transition remains well-described by the two-state approximation. However, the midpoint of the denaturation curve shifts from 4.4 to 5.5 M GuHCl and is accompanied by a 30% increase in the free energy of unfolding, ΔG_{H_2O} (from 3.76 to 4.88 kcal/mol).

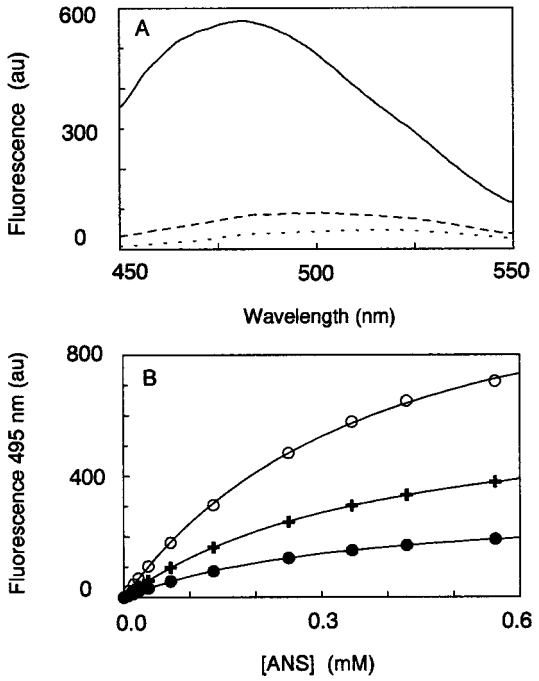

FIGURE 6: Fluorescence emission spectra of free and bound ANS and titration isotherms for ANS binding to Lys^{B29}-myristoylated human insulin measured in 10 mM tris/ClO_4^- buffer, pH 8.0, and 25 °C. Panel A shows emission spectra of samples containing 250 μM ANS recorded using an excitation wavelength of 415 nm in the absence of protein (···), in the presence of 80 μM zinc-free human insulin (- - -) and in the presence of 80 μM Lys^{B29}-myristoylated insulin (—). Panel (B) shows titration curves for the dependence of ANS fluorescence on [ANS] for the titration of (●) 20 μM, (+) 40 μM and (○) 80 μM Lys^{B29}-myristoylated insulin. The solid lines represent fits of the data to eq 3. The following values of the maximum fluorescence change and apparent K_d values for the binding of ANS were obtained: 20 μM protein: $F_{max} = 303$, $K_d = 3.2 \times 10^{-4}$ M^{-1}; 40 μM protein: $F_{max} = 629$, $K_d = 3.5 \times 10^{-4}$ M^{-1}; and 80 μM protein: $F_{max} = 1156$, $K_d = 3.1 \times 10^{-4}$ M^{-1}.

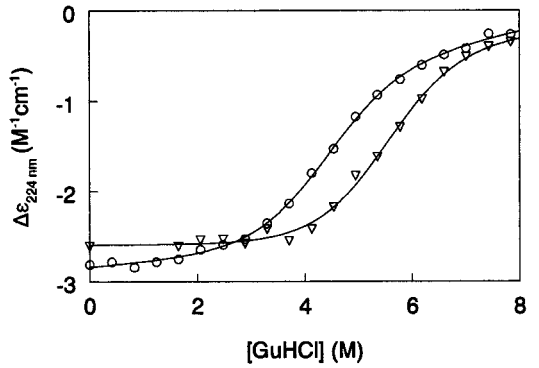

FIGURE 7: GuHCl induced unfolding of 3 μM (○) human insulin and (▽) Lys^{B29}-myristoylated insulin detected by far-UV CD in 10 mM tris/ClO_4^-, pH 8.0. The solid lines represent a least-squares fit of the data to eq 1 using sloping baselines and the following parameters. human insulin: $\Delta G_{H_2O} = 3.76$ kcal mol^{-1}, $m = 0.86$ kcal mol^{-1} M^{-1}, $C_{mid} = 4.37$ M. Lys^{B29}-myristoylated insulin: $\Delta G_{H_2O} = 4.88$ kcal mol^{-1}, $m = 0.89$ kcal mol^{-1} M^{-1}, $C_{mid} = 5.49$ M.

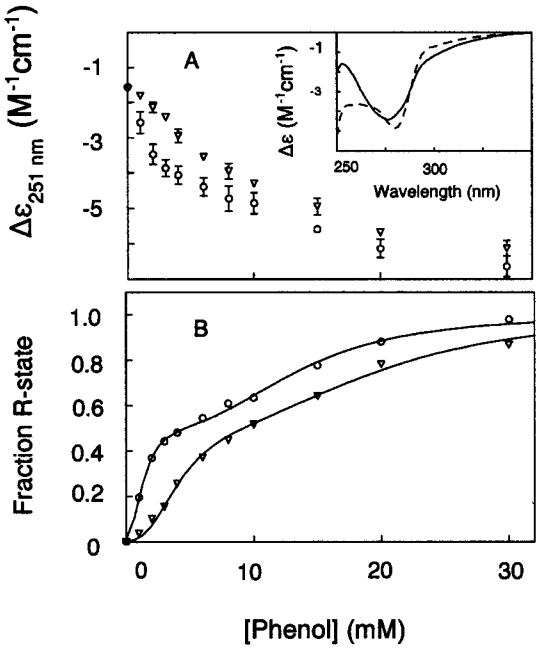

FIGURE 8: CD monitored ligand-induced allosteric interconversions of zinc-hexamers of (○) human insulin and (▽) Lys^{B29}-myristoylated insulin. Panel A shows the CD at 251 nm versus phenol concentration for a 0.6 mM protein solution containing 2 Zn^{2+}/hexamer in 10 mM tris/ClO_4^-, pH 8.0. Insert shows actual NUV−CD spectra for human insulin solutions with 0 and 10 mM phenol, respectively. Panel B shows the fractional CD change at 251 nm as a function of [phenol]. The solid lines represent fits of the data to eq 2 with the following parameters: Human insulin: $L_0^A = 44$, $L_0^B = 5 \times 10^6$, $K_R^0 = 5 \times 10^{-4}$ M^{-1}, $K_R = 2 \times 10^{-4}$ M^{-1}. The corresponding values for Lys^{B29}-myristoylated insulin are $L_0^A = 748$, $L_0^B = 14 \times 10^6$, $K_R^0 = 5 \times 10^{-4}$ M^{-1}, $K_R = 2 \times 10^{-4}$ M^{-1}.

Hexamer Formation and the T to R Transition. In the presence of limited amount of Zn^{2+}, insulin dimers aggregate further into two-zinc insulin hexamers. This aggregate involves a distinct set of protein−protein contacts and the coordination of three His^{B10} imidazolyl groups to each zinc ion. The resulting T_6 hexamer may be converted into the more stable T_3R_3 and R_6 forms by further addition of anionic ligands which bind to the zinc ion and/or phenolic ligands which bind to the hydrophobic pockets in the interface between dimers of T_3R_3 and R_6 hexamers *(14, 23, 24)*. It is shown above that the Lys^{B29}-myristoyl moiety interferes with formation of dimer interface (cf. Figures 2-4). However, the presence of the R_6 insulin hexamer in the crystal structure (Figure 1) predicts that the combined mass action effects of increased protein concentration, the presence of zinc ions and addition of phenolic ligand suffice to displace the myristoyl moiety from the dimer- and hexamer-forming interfaces with resulting formation of a normal hexameric aggregate.

The effect of Lys^{B29}-myristoylation on the thermodynamics of the $T_6 \rightleftarrows T_3R_3 \rightleftarrows R_6$ transitions were evaluated by changes in the near-UV CD spectrum resulting from titration of phenol into 0.6 mM protein solutions containing 2 Zn^{2+}/hexamer in 10 mM Tris/ClO_4^- buffer, pH 8.0. Under these conditions, the T to R conformation change is accompanied by a large change in the 250−260 nm region of the CD spectrum (Figure 8, insert). This change has been used to quantitate the conformational transitions for human insulin (*19*). The 251 nm CD titration profiles in Figure 8A show that the B29-myristoylated species starts out at essentially the same CD value in the absence of phenol as the T_6 human insulin hexamers initially present under these conditions. For both proteins, the addition of phenol leads to a gradual decrease in the CD_{251nm} which tend toward saturation at 30 mM phenol. As expected, the transition for human insulin is clearly biphasic, reflecting that the transformation of T_6 to R_6 takes place via the intermediate T_3R_3 state (*11, 12*). Indeed, the titration profile observed by the 251 nm CD signature closely resembles that obtained by using the UV−vis chromophore 4-hydroxy-3-nitrobenzoate as an indicator (*13*). For the Lys^{B29}-myristoylated species, the decrease in 251 nm CD is somewhat weaker at low phenol concentrations. However, at high [phenol] the CD value approaches that of the native insulin hexamer consistent with the ultimate formation of a R_6 species in solution. The normalized titration isoterms are shown in Figure 8B together with solid lines representing the fit of the data to the three-state allosteric model describing the conformational transitions (*12*). The excellent fit of the data to the model is a further indication that the hexamers formed by Lys^{B29}-acylated insulin retain the ability to undergo the phenol-mediated $T_6 \rightleftarrows T_3R_3 \rightleftarrows R_6$ conversions in solution. In terms of quantitative model parameters, the apparent dissociation constants for phenol binding to the pockets are essentially unchanged by Lys^{B29}-myristoylation. The most significant effect is seen on the allosteric constant for interconversion between T_6 and T_3R_3 forms which is changed about 10−20-fold in the direction of T_6 as a result of the modification. Finally, because the ability of residues B1−B8 to undergo the extended chain to α-helix transition (the T to R transition) positively impacts key stability parameters, we conclude that stable pharmaceutical preparations of Lys^{B29}-myristoylated insulin may be readily formulated.

DISCUSSION

In vivo protein N-myristoylation involves co-translational attachment of myristate catalyzed by the enzyme N-myristoyl transferase which is specific for an N-terminal glycine. The modification is found on both membrane-associated and cytoplasmatic soluble proteins. Although N-myristoylation often plays a role in targeting proteins to membranes, it is generally found that N-myristoylation is required but not sufficient itself for membrane association of proteins, see e.g., ref *25*. Thus, the effects of myristoylation appear more diverse and there is at least three examples where high-resolution structural information is available to help clarify the role played by the myristoyl moiety. One example is the poliovirus, where the X-ray structure reveals a structural role of the myristoyl moiety within the assembled virus particle (*26*). Another example is provided by recoverin which is an N-myristoylated calcium-binding protein present in the retina photoreceptor cells. NMR-studies have shown that the myristoyl moiety of recoverin can switch in a Ca^{2+}-dependent fashion between a form that contacts the protein and a solvated form that is available for use in membrane association (*27−29*). Finally from the large family of protein kinases, the catalytic subunit of protein kinase A is myristoylated in its N-terminal A-helix. The X-ray structure shows that the myristoyl moiety is embedded inside a hydrophobic pocket consisting of the residues of the N-terminus and the catalytic core formed within the large lobe of the structure

(*30*, *31*). Comparison with the structure of the nonmyristoylated species suggests a role for myristate in stabilizing the A-helix with resulting formation of a recognition motif for the phosphorylation site Ser 10 which is part of the A-helix (*32*).

From the examples cited, it appears that a myristoyl group means different things to different N-myristoylproteins. Amino acid sequences necessary for myristoylation of proteins are not known, although the sequence Gly-X-X-X-Ser/Thr may form a consensus sequence for myristoylation, where X represents other amino acids (*26*). Herein, we apply various methods to characterize Lys^{B29}-myristoylated insulin as a model system to examine in detail the structural effects introduced by lipidation. The X-ray structure of Lys^{B29}-myristoylated insulin shows that the R_6 hexamer may be formed in the presence of zinc and phenol and that the constituent monomers retain essentially the structure known from the corresponding R_6 hexamer of human insulin (*8*). Indeed, the only significant effect of the myristoyl moiety is observed in the interaction between hexamers where the fatty acid side chain of one hexamer interacts with the Phe^{B1} side chain of the adjacent hexamer (Figure 1).

The solution studies complement and extend the crystallographic work. While the structure of the polypeptide chains is essentially unchanged, myristoylation of Lys^{B29} modulates key parameters of the insulin molecule in solution. In the monomeric state, the presence of the myristate moiety in the dimer interface leads to modulation of two protein−protein recognition events, i.e., insulin dimerization and receptor binding. Furthermore, the displacement of the myristoyl group from the dimer interface at higher insulin concentrations attest to the flexibility of the position taken up by the fatty acid chain. Nevertheless, the lipid modification results in an 30% increase in stability as expressed by the free energy of unfolding. A stabilizing effect of myristoylation has also been reported in the case of the catalytic subunit of protein kinase A and the regulatory subunit of calcineurin (*33*, *34*). Similarly, depalmitoylation leads to a decrease in the thermal stability of rhodopsin (*35*). The observed effects on stability represent a difference in energy between the folded lipidated protein and the unfolded form wherein the myristoyl group is fully solvated. We conclude that the stabilizing effect of lipidation is general in cases where the lipid moiety becomes partially or fully shielded from the solvent upon attachment to the native protein. The 1.12 kcal/mol increase in folding stability of insulin as a result of myristoylation may be compared with the value of about 0.8 kcal/mol per methylene group for the free energy of transfer from water to a nonpolar solvent of a linear hydrocarbon (*36*). This would correspond to a modest 12% shielding from solvent of the myristate methylene groups when bound to the insulin surface. The relatively high accessibility of the acyl moiety is consistent with the reactivity toward ANS observed in Figure 6.

The presence of Zn^{2+} and phenol drives the formation of hexamers in solution with resulting displacement of the myristoyl moiety from the dimer interface. The position taken up by the acyl side chains under these conditions may or may not be equivalent to that shown in Figure 1. In any event, the titration data in Figure 8 show that the resulting acylated zinc-hexamer retains the ability to undergo the phenol induced conformational transitions in a manner very similar to the $T_6 \rightleftarrows T_3R_3 \rightleftarrows R_6$ scheme established for native insulin hexamers. The myristoylation of Lys^{B29} is not expected to change the structures of the phenolic pockets. Accordingly, the slightly reduced tendency to form T_3R_3 and R_6 states is reflected in the magnitude of the allosteric constants for interconversion between the allosteric states (in particular L_0^A), rather than the dissociation constants for binding of phenol. Whether the acyl group modulates the surroundings of the His^{B10} metal sites in solution remains to be seen.

In conclusion, the well-characterized structure and physical biochemical properties of insulin makes it an attractive model system for analyzing structural effects of protein lipidation. Taken together our studies emphasize the versatility of the myristoyl modification in terms of potential for modulating diverse events such as protein folding, protein−protein interaction as well as ligand induced conformational changes.

ACKNOWLEDGMENT

We thank Dr. I. Jonassen for the provision of Lys^{B29}-myristoylated, des(B30)-insulin, and we thank Susan E. Danielsen, Anne-Marie Kolstrup, and Ane M. Blom for expert technical assistance throughout the course of these studies.

REFERENCES

1. Casey, P. J. (1995) *Science 268*, 221−225.
2. Magee, A. I. (1990) *J. Cell Sci. 97*, 581−584.
3. Chow, M., Der, C. J., and Buss, J. E. (1992) *Curr. Opin. Cell Biol. 4*, 629−636.
4. Ludvigsen, S., Roy, M., Thøgersen, H., and Kaarsholm, N. C. (1994) *Biochemistry 33*, 7998−8006.
5. Olsen, H. B., Ludvigsen, S., and Kaarsholm, N. C. (1996) *Biochemistry 35*, 8836−8845.
6. Kaarsholm, N. C., Norris, K., Jørgensen, R. J., Mikkelsen, J., Ludvigsen, S., Olsen, O. H., Sørensen, A. R., and Havelund, S. (1993) *Biochemistry 32*, 10773−10778.
7. Baker, E. N., Blundell, T. L., Cutfield, J. F., Cutfield, S. M., Dodson, E. J., Dodson, G. G., Hodgkin, D. C., Hubbard, R. E., Isaacs, N. W., Reynolds, C. D., Sakabe, K., Sakabe, N., and Vijayan, N. M. (1988) *Philos. Trans. R. Soc. Ser. B. Biol. Sci. 319*, 369−456.
8. Derewenda, U., Derewenda, Z., Dodson, E. J., Dodson, G., Reynolds, C. D., Smith, G. D., Sparks, C., and Swensen, D. (1989) *Nature 338*, 594−596.
9. Smith, G. D., Swenson, D. C., Dodson, E. J., Dodson, G. G., and Reynolds, C. D. (1984) *Proc. Natl. Acad. Sci. U.S.A. 81*, 7093−7097.
10. Kaarsholm, N. C., Ko, H.-C., and Dunn, M. F. (1989) *Biochemistry 28*, 4427−4435.
11. Brzovic, P. S., Choi, W. E., Borchardt, D., Kaarsholm, N. C., and Dunn, M. F. (1994) *Biochemistry 33*, 13057−13069.
12. Bloom, C. R., Choi, W. E., Brzovic, P. S., Ha, J. J., Huang, S.-T., Kaarsholm, N. C., and Dunn, M. F. (1995) *J. Mol. Biol. 245*, 324−330.
13. Bloom, C. R., Wu, N., Dunn, A., Kaarsholm, N. C., and Dunn, M. F. (1998) *Biochemistry 37*, 10937−10944.
14. Rahuel-Clermont, S., French, C. A., Kaarsholm, N. C., and Dunn, M. F. (1997) *Biochemistry 36*, 5837−5845.
15. Markussen, J., Havelund, S., Kurtzhals, P., Andersen, A. S., Halstrøm, J., Hasselager, E., Larsen, U. D., Ribel, U., Vad, K., and Jonassen, I. (1996) *Diabetologia 39*, 281−288.
16. Whittingham, J. L, Havelund, S., and Jonassen, I. (1997) *Biochemistry 36*, 2826−2831.
17. Pace, C. N. (1975) *CRC Crit. Rev. Biochem 3*, 1−43.
18. Santoro, M. M., and Bolen, D. W. (1988) *Biochemistry 27*, 8063−8068.

19. Krüger, P., Gilge, G., Cabuk, Y., and Wollmer, A. (1990) *Biol. Chem. Hoppe-Seyler 371*, 669−673.
20. Bloom, C. R., Kaarsholm, N. C., Ha, J., and Dunn, M. F. (1997) *Biochemistry 36*, 12759−12765.
21. Kurtzhals, P., Havelund, S., Jonassen, I., Kiehr, B., Larsen, U. D., Ribel, U., and Markussen, J. (1995) *Biochem. J. 312*, 725−731.
22. Stryer, L. (1965) *J. Mol. Biol. 13*, 482−495.
23. Smith, G. D., and Ciszak, E. (1994) *Proc. Natl. Acad. Sci. U.S.A. 91*, 8851−8855.
24. Ciszak, E., and Smith, G. D. (1994) *Biochemistry 33*, 1512−1517.
25. Resh, M. D. (1999) *Biochim. Biophys. Acta 1451*, 1−16.
26. Chow, M., Newman, J. F. E., Filman, D., Hogle, J. M., Rowlands, D. J., and Brown, F. (1987) *Nature 327*, 482−486.
27. Hughes, R. E., Brzovic, P. S., Klevit, R. E., and Hurley, J. B. (1995) *Biochemistry 34*, 11410−11416.
28. Takana, T., Ames, J. B., Harvey, T. S., Stryer, L., and Ikura, M. (1995) *Nature 376*, 444−447.
29. Ames, J. B., Tanaka, T., Ikura, M., and Stryer, L. (1995) *J. Biol. Chem. 270*, 30909−30913.
30. Karlsson, R., Zheng, J., Xuong, N.-H., Taylor, S. S., and Sowadski, J. M. (1993) *Acta Crystallogr., Sect. D 49*, 381−388.
31. Zheng, J., Knighton, D. R., Xuong, N. H., Taylor, S. S., Sowadski, J. M., and Ten Eyck, L. F. (1993) *Protein Sci. 2*, 1559−1573.
32. Sowadski, J. M., Ellis, C. A., and Madhusudan (1996) *J. Bioenerg. Biomembr. 28*, 7−12.
33. Yonemoto, W., Mcglone, M. L., and Taylor, S. S. (1993) *J. Biol. Chem. 268*, 2348−2352.
34. Kennedy, M. T., Brockman, H., and Rusnak, F. (1996) *J. Biol. Chem. 271*, 26517−26521.
35. Traxler, K. W., and Dewey, T. G. (1994) *Biochemistry 33*, 1718−1723.
36. Jencks, W. P. (1969) *Catalysis in Chemistry and Enzymology*, Mcgraw-Hill, New York.

BI001201I